OPEN ACCESS
OPUS AUGSBURG

Universität Augsburg
Universitätsbibliothek

An ECG simulator for generating maternal-foetal activity mixtures on abdominal ECG recordings

Joachim Behar, Fernando Andreotti, Sebastian Zaunseder, Qiao Li, Julien Oster, Gari D. Clifford

Angaben zur Veröffentlichung / Publication details:

Behar, Joachim, Fernando Andreotti, Sebastian Zaunseder, Qiao Li, Julien Oster, and Gari D. Clifford. 2014. "An ECG simulator for generating maternal-foetal activity mixtures on abdominal ECG recordings." *Physiological Measurement* 35 (8): 1537–50. https://doi.org/10.1088/0967-3334/35/8/1537.

Nutzungsbedingungen / Terms of use: **CC BY-NC-ND 4.0**

Dieses Dokument wird unter folgenden Bedingungen zur Verfügung gestellt: / This document is made available under these conditions:
CC-BY-NC-ND 4.0: Creative Commons: Namensnennung - Nicht kommerziell - Keine Bearbeitung
Weitere Informationen finden Sie unter: / For more information see:
https://creativecommons.org/licenses/by-nc-nd/4.0/deed.de

An ECG simulator for generating maternal-foetal activity mixtures on abdominal ECG recordings

Joachim Behar[1], Fernando Andreotti[1,2], Sebastian Zaunseder[2], Qiao Li[1], Julien Oster[1] and Gari D Clifford[1,3]

[1] Institute of Biomedical Engineering, Department of Engineering Science, University of Oxford, Oxford OX1 3PJ, UK
[2] Institute of Biomedical Engineering, Faculty of Electrical and Computer Engineering TU Dresden, Helmholtzstr. 10, 01069 Dresden, Germany
[3] Departments of Biomedical Informatics & Biomedical Engineering, Emory University & Georgia Institute of Technology, Atlanta, GA USA

E-mail: joachim.behar@eng.ox.ac.uk

Abstract

Accurate foetal electrocardiogram (FECG) morphology extraction from non-invasive sensors remains an open problem. This is partly due to the paucity of available public databases. Even when gold standard information (i.e derived from the scalp electrode) is present, the collection of FECG can be problematic, particularly during stressful or clinically important events.

In order to address this problem we have introduced an FECG simulator based on earlier work on foetal and adult ECG modelling. The open source foetal ECG synthetic simulator, *fecgsyn*, is able to generate maternal-foetal ECG mixtures with realistic amplitudes, morphology, beat-to-beat variability, heart rate changes and noise. Positional (rotation and translation-related) movements in the foetal and maternal heart due to respiration, foetal activity and uterine contractions were also added to the simulator.

The simulator was used to generate some of the signals that were part of the 2013 PhysioNet Computing in Cardiology Challenge dataset and has been posted on Physionet.org (together with scripts to generate realistic scenarios) under an open source license. The toolbox enables further research in the field and provides part of a standard for industry and regulatory testing of rare pathological scenarios.

Keywords: non invasive foetal ECG, dipole model, synthetic ECG, heart rate variability, contraction, foetal movement

1. Introduction

Despite significant advances in the clinical analysis of adult electrocardiogram (ECG), signal processing techniques and the computational power of digital processors, the analysis of non-invasive foetal ECGs (NI-FECG) is still a challenge. The PhysioNet/Computing in Cardiology Challenge 2013 ('the Challenge') (Silva *et al* 2013, Clifford *et al* 2014) partially addressed these limitations by making a set of NI-FECG data publicly available to the scientific community for evaluation of signal processing techniques. This database consists of 447, one-minute abdominal signals, making it the largest publicly available dataset for NI-FECG signal processing to date. Despite the advancements in the field of NI-FECG signal processing that the Challenge facilitated, there were a number of limitations concerning the available data. One of the main limitations (aside from the limited number of channels of maternal and fetal data available) was the absence of pathological cases (pregnancy with adverse outcome) or rare cases such as similar foetal (FHR) and maternal heart rates (MHR) at times of abrupt heart rate changes. This motivated the development of an artificial NI-FECG simulator and inclusion of a limited number of artificially generated signals into the challenge database (20 in total) in order to model some of these events.

An artificial FECG-maternal ECG (MECG) mixture simulator can be used for creating realistic abdominal recordings that model specific physiological phenomena. The simulator presented in this work, *fecgsyn*, is an extension of the ECG simulator introduced by McSharry *et al* (2003), later adapted by Sameni *et al* (2007) to reflect a single dipole per cardiac source. By decreasing the dipole magnitude and placing it at a certain location with respect to the maternal heart, a foetal-maternal mixture is generated. The dipole model is linearly related to the body surface potentials by a projection matrix that takes into account the temporal movements and rotations of the cardiac dipole. By superimposing two such projections with different amplitudes it is possible to simulate a realistic FECG-MECG mixture. However, several features of the mixing were not implemented in the previously published simulator. In particular, the non-stationary mixing due to respiration and foetal movement, as well as realistic heart rate changes (both normal and pathological) were not included in previous simulators.

This article introduces the physiological phenomena encompassed by the simulator, and the framework for generating the foetal-maternal mixtures on the abdominal ECG. Some specific cases are then described and simulated. Finally, a summary of limitations and possible future additions to the simulator are presented.

2. Simulator description

2.1. Simulator overview

Surface electrodes measure the electrical potential created by different sources that propagate throughout the volume conductor. These sources can be categorised as cardiac sources (i.e. maternal and foetal myocardia) or noise sources (e.g. muscle activity from movement or contractions). The developed simulator considers all sources as point source dipoles, that may be rotated and translated. The dipoles have two basic attributes: a vector, represented by three coordinates in the Cartesian coordinates system, and a location which, together with the electrodes' location, define the propagation matrix of the signals to the observation points. Table 1 lists the key parameters together with the physiological effects that were modelled. Figure 1 illustrates the modelling of the volume conductor (defined as a cylinder), foetal and

Table 1. Important simulator parameters.

	Parameters	Definition	Range/type
	fs	sampling frequency (Hz)	—
NS	*ntype*	type of noise	MA, EM, BW (Moody *et al* 1984)
	SNR_{fm}	signal to noise ratio of the FECG relative to maternal interference	—
	SNR_{mn}	signal to noise ratio of the MECG relative to noise	—
HR	*mhr*	maternal heart rate (bpm)	70–140 bpm
	fhr	foetal heart rate (bpm)	120–160 bpm (von Steinburg *et al* 2012)
	macc	maternal acceleration/deceleration (bpm)	—
	facc	foetal acceleration/deceleration (bpm)	—
	macctype/facctype	maternal/foetal acceleration/deceleration type	'none', 'nsr', 'tanh', 'mexhat', 'gauss'
TR	*ftraj*	foetal heart trajectory to model foetal movement	'none', 'linear', 'spline', 'helix'
RS	*mres*	maternal respiration frequency	0.2–0.3 Hz
	fres	foetal respiration frequency	0.8–0.95 Hz (Dornan *et al* 1984)
GE	*mheart*	maternal heart position in polar coordinates	—
	fheart	foetal heart position in polar coordinates	—
	elpos	electrode position in polar coordinates	—
	mvcg	maternal vectorcardiogram number	1–9
	fvcg	foetal vectorcardiogram number	1–9
EB	*mectb*	ectopic beat for the maternal ECG	boolean
	fectb	ectopic beat for the foetal ECG	boolean

Note: NS, noise; HR, heart rate; TR, trajectory; RS, respiration; GE, geometry; MA, muscle artifact; EM, electrode motion; BW, baseline wander; EB, ectopic beat.

maternal heart locations, as well as the electrode positions. The dipole frame is represented by three arrows (that depict the orientation of the foetal and maternal body axis), centred on each of the maternal and foetal heart. Table 2 specifies the heart and electrode locations in polar coordinates (with θ the angle (in rad), ρ the radius and z the height), used for the illustration on figure 1. The following phenomena, that affect the morphology and dynamics of the abdominal ECG, were modelled: noise (muscle noise, electrode motion, baseline wander), maternal respiration and foetal breathing movement, foetal movement, contractions, presence of ectopic beats and multiple pregnancies.

2.2. The dipole model

Following the work of Sameni *et al* (2007) the myocardial electrical activity is represented by a time-varying vector which has its origin at the centre of the heart. The dipole vector can be written as $\underline{\mathbf{d}}(t) = x(t)\,\underline{\mathbf{e}}_x + y(t)\,\underline{\mathbf{e}}_y + z(t)\,\underline{\mathbf{e}}_z$, where $\underline{\mathbf{e}}_j$, $j \in \{x, y, z\}$, are basis vectors of the body axis. The torso potential, $\phi(t)$, generated by the dipole and sensed by an electrode located at a point, such as the vector from the dipole center to this point, is defined by $\underline{\mathbf{r}}$, and can be written as:

$$\phi(t) = \frac{\underline{\mathbf{d}}(t)\cdot\underline{\mathbf{r}}(t)}{4\pi\sigma|\underline{\mathbf{r}}(t)|^3} = \frac{1}{4\pi\varepsilon_0}\left[x(t)\frac{r_x(t)}{|\underline{\mathbf{r}}(t)|^3} + y(t)\frac{r_y(t)}{|\underline{\mathbf{r}}(t)|^3} + z(t)\frac{r_z(t)}{|\underline{\mathbf{r}}(t)|^3}\right]. \quad (1)$$

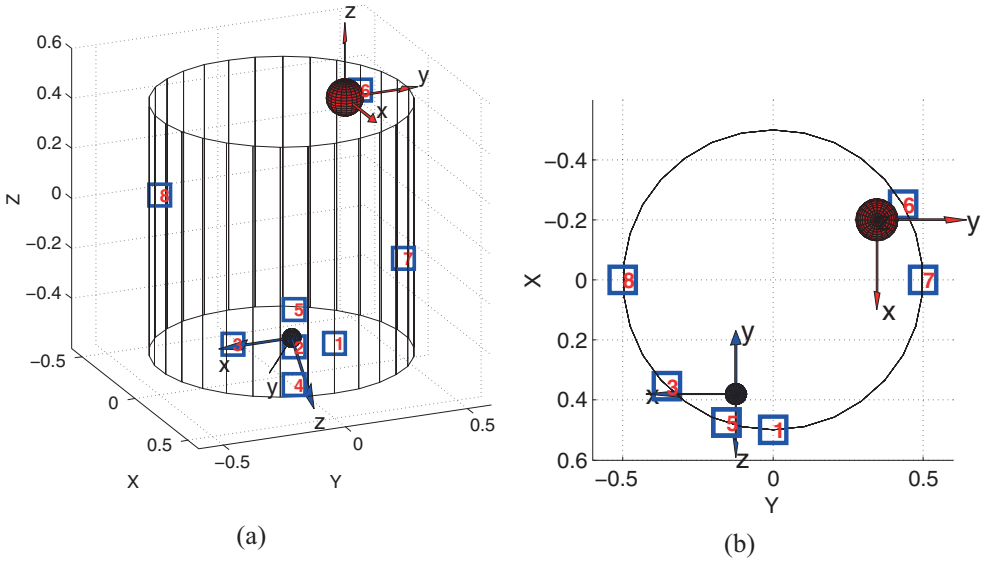

Figure 1. (*a*) Volume conductor representation. The two spheres represent maternal (large sphere) and the foetal (smaller sphere) hearts. The blue numbered squares show the location of the electrodes on the volume conductor, while the arrows represent the orientation of the foetal and maternal body axis which are defined by the heart orientation; (*b*) top view of the volume conductor.

Table 2. Electrodes' and hearts' positions for the example in figure 1; θ the angle (in rad), ρ the radius and z the height in cylindrical coordinates.

Electrode Variable	1	2	3	4	5	6	7	8	*fheart*	*mheart*
θ	0	$-\pi/10$	$-\pi/4$	$-\pi/10$	$-\pi/10$	$2\pi/3$	$\pi/2$	$3\pi/2$	$2\pi/3$	$-\pi/10$
ρ	0.50	0.50	0.50	0.50	0.50	0.50	0.50	0.50	0.40	0.40
z	−0.30	−0.30	−0.3	−0.45	−0.15	0.40	−0.20	0.20	0.40	−0.30

where ε_0 is the permittivity of the volume conductor (here, considered to be isotropic and unitary). The tension measured at this electrode is then given by $\phi(t) - \phi_0(t)$, where $\phi_0(t)$ is the reference potential, which was taken to be located on the back of the cylinders at the polar coordinates [0.5-0.3]. Note that the potential is time dependent with respect to $\underline{\mathbf{d}}(t)$ and $\underline{\mathbf{r}}(t)$ which can vary with foetal movement and respiration, for example.

2.3. The ECG model

In order to generate realistic MECG and FECG waveforms, the dynamical ECG model introduced by McSharry *et al* (2003) was used. The model is built on the premise that a set of Gaussian kernel functions can be used to approximate ECG cycles. Figure 2 illustrates how an ECG cycle is approximated by a set of $N = 7$ Gaussian functions. The set of equations that describes the model can be written:

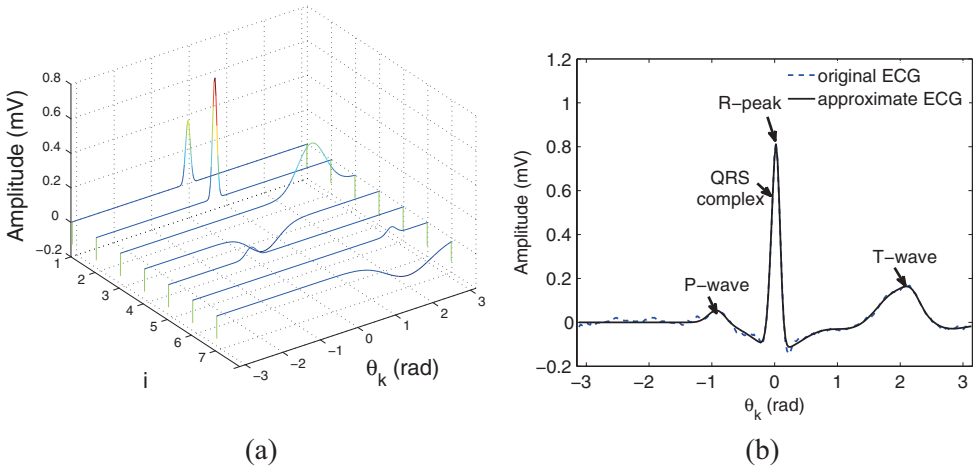

Figure 2. (*a*) The seven Gaussians (index i) used to represent an ECG cycle. (*b*) Original ECG cycle (dotted line) and the reconstructed ECG cycle obtained by summing the seven Gaussian functions from (*a*).

$$\begin{cases} \dot{\theta} = \omega \\ \dot{x} = -\sum_{i=1}^{N} \dfrac{\alpha_i^x \omega}{(b_i^x)^2} \Delta\theta_i^x \exp\left(-\dfrac{(\Delta\theta_i^x)^2}{2(b_i^x)^2}\right) \\ \dot{y} = -\sum_{i=1}^{N} \dfrac{\alpha_i^y \omega}{(b_i^y)^2} \Delta\theta_i^y \exp\left(-\dfrac{(\Delta x\theta_i^y)^2}{2(b_i^y)^2}\right) \\ \dot{z} = -\sum_{i=1}^{N} \dfrac{\alpha_i^z \omega}{(b_i^z)^2} \Delta\theta_i^z \exp\left(-\dfrac{(\Delta\theta_i^z)^2}{2(b_i^z)^2}\right), \end{cases} \tag{2}$$

with $\Delta\theta_i^j \equiv \left(\theta - \xi_i^j\right) \bmod 2\pi$, $j \in \{x, y, z\}$, where α_i^j, b_i^j, ξ_i^j correspond to the peak amplitude, width and centre parameters of the ith Gaussian kernel functions respectively. The velocity of the circular trajectory of the heart dipole $\underline{\mathbf{d}}(t)$ is $\omega = 2\,\pi\,f$, with f being the beat-to-beat heart rate (in Hz). The model parameters for the FECG-MECG mixture were derived from a set of vectorcardiograms (VCGs)[4] from the PTB Diagnostic ECG Database (Bousseljot *et al* 1995) records (i.e. α_i^j, b_i^j, ξ_i^j parameters were derived for all three channels of the VCGs). For each cardiac signal, heart rate variability (HRV) is introduced by making ω time variant. This allows the production of maternal and foetal signals in both physiological and pathological scenarios; important for testing robustness of NI-FECG extraction techniques. Moreover, since each dipole is independent from the others, more than one foetal heart dipole can be generated to simulate multiple pregnancies. Additionally, by changing the signal-to-noise ratio between the maternal and foetal signal (SNR_{fm}), different mixtures with different FECG amplitudes can be generated.

2.4. Forward propagation of the dipoles fields

A projection matrix built upon the cardiac dipole model (equation (1)) was used to project the VCG waveforms onto the electrode positions on the surface of the volume conductor, therefore

[4] The parameters were extracted from the following records: s0273lre, s0291lre, s0302lre, s0303lre, s0306lre, s0491_re, s0533_re from the PTBDB and two others sets of parameters were taken from Sameni *et al* (2007).

obtaining ECG signals. The projection matrix contains information about the permittivity of the conductor (assumed constant), dipole origin and relative location between observing electrodes and source. For the projection of a single dipole, mathematically we formulate

$$\underline{\mathbf{s}}(t) = \mathbf{H}(t) \cdot \mathbf{R}(t) \cdot \underline{\mathbf{d}}(t) + \underline{\mathbf{w}}(t), \tag{3}$$

where $\underline{\mathbf{s}}(t) \in \Re^M$ corresponds to the signal recorded on the M ECG channels at time t, $\underline{\mathbf{d}}(t) = [x(t), y(t), z(t)]^T$ contains the three components of the dipole vector generated by the ECG model (McSharry *et al* 2003), $\mathbf{H}(t) \in \mathrm{R}^M$ corresponds to the body volume conductor model (projection matrix) which is time-varying in cases where the dipole is translated along a given trajectory, $\mathbf{R}(t) \in \Re^{3 \times 3}$ is the rotation matrix for the dipole vector, and $\underline{\mathbf{w}}(t) \in \Re^M$ corresponds to the noise on each ECG channels at time t. Allowing the projection matrix $\mathbf{H}(t)$ to be time-variant opens new possibilities for translating dipoles, which are useful when modelling breathing-related heart motion and foetal activity-related movement. The resulting signals are given by

$$\underline{\mathbf{s}}(t) = \mathbf{H}_m(t) \cdot \mathbf{R}_m(t) \cdot \underline{\mathbf{d}}_m(t) + \mathbf{H}_f(t) \cdot \mathbf{R}_f(t) \cdot \underline{\mathbf{d}}_f(t) + \underline{\mathbf{w}}(t), \tag{4}$$

where the subscripts m and f indicate mother and foetus respectively. The forward projection matrices can be written as $\mathbf{H}_m = \left(h_{ij}^m\right)$, $\mathbf{H}_f = \left(h_{ij}^f\right)$ with $j \in \{x, y, z\}$ and i representing the electrode number so that:

$$h_{ij}(t) = \frac{1}{4\pi\varepsilon_0} \frac{r_j^i(t)}{|\underline{\mathbf{r}}^i(t)|^3},$$

where ε_0 is the permittivity of the volume conductor, $\underline{\mathbf{r}}^i$ is the vector going from the dipole to ith electrode and r_j^i is the jth component of $\underline{\mathbf{r}}^i$. Note that the elements of the $\mathbf{H}$ matrices are time dependent.

2.5. Modelling noise

Real noise signals from the PhysioNet Noise Stress Test Database (Goldberger *et al* 2000, Moody *et al* 1984) (NSTDB) were used. The NSTDB contains 30 min, two-channel recordings of three noise sources: motion artifact (MA), electrode motion (EM) and baseline wander (BW). However there are three main limitations when using these records: (1) their length is limited to 30 min (thus sub-segments of these records would be re-used if the modelled signal has a greater length), (2) there are only two channels available (if we want to model a noise dipole we need three orthogonal components) and (3) this is noise from one individual, thus not accounting for inter-individuals variability. In order to tackle these limitations we propose to use an auto-regressive (AR) model to simulate the non-stationarity of the noise process.

The coefficients of the AR model were estimated over a randomly selected 20 s segment of one of the NSTDB signals. This defined the AR filter's coefficients, associated poles and frequency response. In order to account for the uniqueness of the records available in the NSTDB and incorporate some variability, the poles from the identified AR filter were left to evolve slightly, following a random walk, while ensuring they stayed in the unit circle (ensuring the stability of the filter), and preserving symmetry between conjugated poles. In order to generate a third noisy channel, principal component analysis (PCA) was applied to both of the generated noise channels, with the first principal component considered to be the third channel. This ensures that the generated channel was not independent from the original two channels. Indeed the VCG is based on the concept of the dipole to approximate the electromagnetic activity of the heart. It uses orthogonal leads with the idea that the three VCG leads are independent in the second order sense (i.e. uncorrelated). However in practice this is an approximation

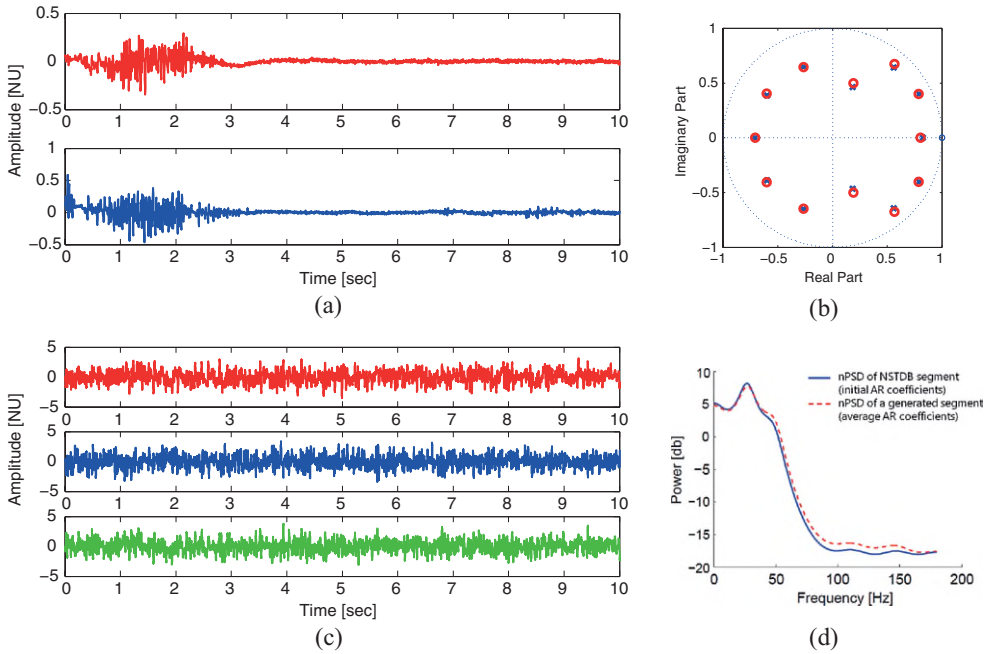

Figure 3. Noise generator. (*a*) Noisy segment selected in the MA record of the NSTDB (2 channels available); (*b*) the AR coefficients (initial value: blue crosses and final values after leaving the coefficient evolve following a random walk: red circle); (*c*) artificially generated noise (the third channel corresponds to the first principal component of PCA applied on the first two channels), (*d*) the normalised power spectral density (nPSD) of the second channels of the NSTDB selected noise and the second generated noise channel.

because the VCG channels are to some extent correlated and not independent in a higher order sense. In the same way the channels of the, VCG-like of the noise dipole, will exhibit some dependence (in a higher order sense). This is an approximation that is realistic given that muscle recorded on different parts of the body will likely not be completely independent.

Figure 3 illustrates a noisy segment from the MA record of the NSTDB, and the artificially generated noise together with the normalised power spectral density (nPSD) . The nPSD was obtained by computing the frequency response from the transfer function having the initial AR coefficients (for obtaining the nPSD of the NSTDB segment) and the averaged evolving AR coefficients (for obtaining the nPSD of the generated segment). Note how the nPSD shape was preserved while producing the artificial noisy segments.

2.6. Signal calibration

Cardiac and noise signals were calibrated in a similar fashion with respect to the maternal signal. The amplitude scaling gain, p, applied to foetal or noise signals before adding them to the signal mixture, is defined as

$$y(t) = x(t) + p \cdot v(t) \tag{5}$$

$$p = \sqrt{\frac{P_x}{P_v}} \cdot 10^{\frac{-S}{20}} \tag{6}$$

where S represents the SNR in decibels of the signal to be calibrated (i.e. $-\text{SNR}_{fm}$ or SNR_{mn}), $y(t)$ is the output signal (i.e. the abdominal mixture $\underline{\mathbf{s}}$), $x(t)$ is the maternal signal and $v(t)$ is either the foetal signal (for $S = -\text{SNR}_{fm}$) or noise (for $S = \text{SNR}_{mn}$). P_x represents the power of the MECG and P_v the power of noise/foetal signal. In order to eliminate the influence of baseline wander from the MA and EM records on the P_v calculation, these were high-pass filtered by a 10th order zero-phase Butterworth filter at 1 Hz cut-off frequency prior this calculation. Filtering was performed because the MA and EM records contained BW noise which usually has a high power (which would be taken into account when computing P_v) but is easier to remove than MA or EM noise.

Foetal calibration was performed as follows: the average power of the MECG and FECG projected onto the abdominal channels were computed. Given these averaged power and the SNR_{fm}, the coefficient p from equation (6) was computed and the resulting mixture was obtained using equation (5) for each individual channel. With respect to noise, any subset of the MA, EM, BW noises can be added to the abdominal mixture in a similar way. In the presence of multiple noise types, the parameter SNR_{mn} specified the overall amount of noise to add to the MECG.

2.7. Modelling respiration

Respiration influences the morphology of the electrocardiogram by changing the position of the heart, but also the orientation of the cardiac dipole. The respiratory pattern was modelled as a variable sawtooth-like signal, $\beta(t)$. The respiration model was introduced in Stridh and Sornmo (2001) then applied in Petrenas *et al* (2012) for simulating f-waves in the ECG. In this work, the first three coefficients of the Fourier transform of the normalised sawtooth signal were used to model the waveform while time-varying amplitude and frequency modulation was also introduced in order to account for the non-stationary behaviour of the physiological process. The model can be written as:

$$\beta(t) = \sum_{j=1}^{3} a_j(t)\ \sin\left(j\omega_0 t + \frac{\Delta f_d}{f_m}\sin\left(\omega_m t\right)\right),$$

$$a_j(t) = \frac{2}{j\pi}\left(a + \Delta a\ \sin\left(\omega_a t\right)\right),$$

where $\omega_0 = 2\,\pi f_0$ is the fundamental angular frequency corresponding to the breathing rate, Δf_d is the frequency deviation tolerated around f_0, f_m is the modulation frequency (i.e. frequency at which the breathing wave is modulated), a is the sawtooth amplitude, Δa is the modulation amplitude and $\omega_a = 2\,\pi f_a$ with f_a is the modulation frequency. For the simulations in this work the values were set to: $\Delta a = 0.3$, $f_a = 0.1$ Hz, $\Delta f_d = 0.05$ Hz and $f_m = 0.1$ Hz. Typical breathing rates are between 12 and 18 breaths per minute (brpm) for adults and $\sim$ 50 brpm for a foetus[5]. Figure 4 shows an example of the respiratory waveform generated over a 15 s period. The sawtooth-like function models respiration as a slowly increasing inspiration and rapidly declining expiration. The time-varying rotation matrix coupled with the breathing waveform was then computed using the following equations:

[5] Numerical values on healthy foetuses as found by Dornan *et al* (1984) were 57.2 (30–33 weeks of gestation) and 47.9 brpm (37–40 weeks). Note that the foetus does not actually breath as the oxygen supply is coming from the mother. However breathing movement is observed for the foetus after 10 weeks of gestation (Greer 2012).

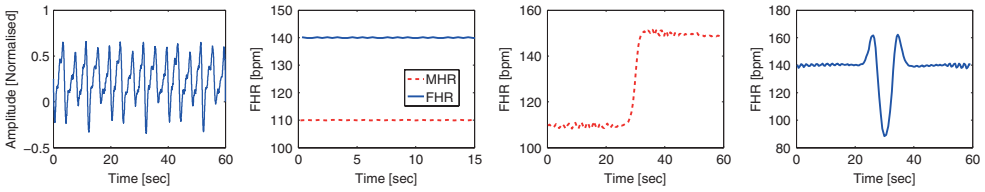

Figure 4. Example of simulated (*a*) respiration waveform; (*b*) heart rate; (*c*) fast heart rate increase; (*d*) umbilical cord effect on FHR.

$$\psi_j = \psi_j^{max} \cdot \beta(t) + \psi_j^0,$$

$$\mathbf{R}(t) = \mathbf{R}_x(t) \cdot \mathbf{R}_y(t) \cdot \mathbf{R}_z(t)$$

$$= \begin{bmatrix} 1 & 0 & 0 \\ 0 & \cos(\psi_x) & \sin(\psi_x) \\ 0 & -\sin(\psi_x) & \cos(\psi_x) \end{bmatrix} \begin{bmatrix} \cos(\psi_y) & 0 & \sin(\psi_y) \\ 0 & 1 & 0 \\ -\sin(\psi_y) & 0 & \cos(\psi_y) \end{bmatrix} \begin{bmatrix} \cos(\psi_z) & \sin(\psi_z) & 0 \\ -\sin(\psi_z) & \cos(\psi_z) & 0 \\ 0 & 0 & 1 \end{bmatrix}$$

with $\beta(t)$ representing the sawtooth shape of the generated signal, ψ_j the rotation angle around axis j with $j \in \{x, y, z\}$, and ψ_j^0 the static (mean) orientation of the foetal heart with respect to the maternal heart (which is assumed to be aligned with the default Cartesian basis). Note that ψ_j is time dependent but for notation simplicity the time index was omitted. $\psi_j^{\max}$ is the maximum deviation of the rotation angle ψ_j in radians and taken to be $\psi_x^{\max} = 0.2$, $\psi_y^{\max} = 0.16$, $\psi_z^{\max} = 0.14$ (order of magnitude inspired by Leanderson *et al* (2003)).

The same sawtooth function was used to modulate the translation of the heart during breathing. According to (McLeish *et al* 2002) the heart position oscillates around 1–2 cm along the z-axis with the breathing activity of the diaphragm. We approximated this range by allowing the heart to translate its position by 5% of the height of the cylinder volume conductor for the maternal heart and 1.5% for the foetal heart.

2.8. Modelling heart rate variability

The model for HRV introduced by McSharry *et al* (2003) was used. The sympatho-vagal balance is defined as the balance between the effect of the sympathetic and parasympathetic nervous systems which act in opposite directions. The sympatho-vagal balance is believed to be reflected in the beat-to-beat changes of the cardiac cycle Malik and Camm (1995). The RR time series power spectrum was modelled as a mixture of two Gaussians. The first one models the HR modulation with respiration (parasympathetic activity) known as respiratory sinus arrhythmia (RSA, ~ 0.25 Hz for adults), and the second one models the Mayer peak for baroreflex regulation (sympathetic activity, ~ 0.1 Hz). Figure 4(*b*) shows two HR time series (one for the FHR and one for MHR) generated using this model. Usage of this model is referred to as normal sinus rythm (NSR) modulation. Furthermore, two additional heart rate related effects were modelled: (1) a rapid decrease or increase of HR that models fast transition to prolonged deceleration caused by foetal head compression or uteroplacental insufficiency (Feinstein *et al* 1993) and (2) the ischemic response due to umbilical cord compression. The first effect was modelled using a hyperbolic tangent increase or decrease in HR, while the latter was modelled using a 'Mexican-hat' function to modulate the FHR. The 'Mexican hat' function in the one-dimensional case is defined as:

$$f(t) = \frac{2}{\sqrt{3\sigma}\,\pi^{\frac{1}{4}}}\left(1-\frac{t^2}{\sigma^2}\right)\exp\left(-\frac{t^2}{2\sigma^2}\right),$$

where t is the time index and σ the standard deviation. Figure 4(d) shows an example of modelled FHR response to umbilical cord compression; the umbilical cord is initially only slightly compressed—there is partial obstruction of the umbilical vein. This results in an increase of heart rate. As the obstruction increases the umbilical artery becomes occluded resulting in a decrease of FHR thus creating a 'shoulder' followed by a drop. As the umbilical cord is released, there is a FHR recovery with a possible slight increase before going back to the baseline value (second shoulder) (Patterns 1999).

2.9. Modelling foetal movement

Foetal movements were simulated by changing the position of the cardiac dipole within the volume conductor. This makes the projection matrix time variant since the distance between dipole and electrodes changes at every time instant. Different trajectory patterns were modelled, including linear, spline and helix (see table 1).

2.10. Modelling contractions

Uterine contractions are muscular activities that vary in intensity and periodicity during pregnancy. By using the MA noise model (section 2.5) and modulating it by an envelope function (e.g. Gaussian) for simulating contraction's intensity increase and decay, we are able to produce a realistic estimate on the contraction signals. Umbilical cord compression might happen during a uterine contraction, with this compression generating a typical FHR pattern, modelled using the Mexican-hat function described in section 2.8. With the developed model, early and late decelerations can be modelled by time shifting the HRV and noise modulating functions. Early deceleration corresponds to the FHR going below the baseline heart rate. In general the onset, minimum and recovery of the deceleration are in phase with the onset, peak and recovery of the contraction. In the case of a late deceleration, the onset, minimum and recovery of the deceleration happen after the contraction (Feinstein *et al* 1993). Examples are depicted in figure 5. During those episodes, it is possible that a cross-over between MHR and FHR occurs which might make the extraction of the FECG more difficult.

2.11. Modelling ectopic beats

Ventricular ectopic beats or premature ventricular contractions (PVC) occur commonly, even in healthy individuals (Sobotka *et al* 1981). According to Kennedy *et al* (1985) ectopic beats occur in 1% of normal patients submitted to standard ECG measurements and in 40–75% of the patients assessed by Holter ECG (during 24 or 48 h). The consequences of these beats and arrhythmia for both mother and foetus are rarely analysed in NI-FECG literature. The model used was introduced by Clifford *et al* (2010) and subsequently used in Oster and Clifford (2013). It makes use of a Hidden Markov Model to switch between normal and ectopic beats. The state transition matrix ($\mathbf{T}$) is described as:

$$\mathbf{T} = \begin{bmatrix} rn & 1-rn \\ 1-re & re \end{bmatrix}$$

where $rn = 0.7 + 0.1 \cdot \mathcal{U}(0,\ 1)$ is the probability of the incoming beat to be chosen as normal given that the previous beat was normal and $re = 0.2 + 0.1 \cdot \mathcal{U}(0,\ 1)$ is the probability of the

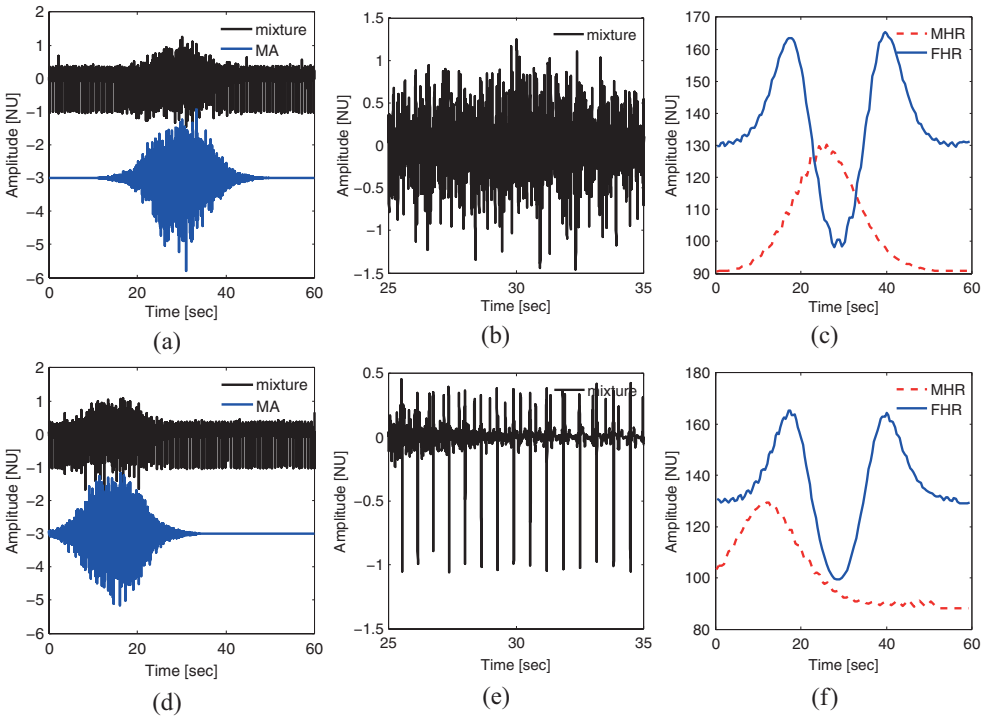

Figure 5. (*a*) FECG-MECG mixture (60 s) with a contraction in the centre; (*b*) 10 s excerpt from (*a*); (*c*) the corresponding FHR and MHR for plots (*a*), representing an early deceleration; (*d*) signal mixture (60 s) with a contraction at the beginning of simulation; (*e*) 10 s segment from (*d*); (*f*) is the corresponding FHR and MHR for plots (*d*), representing a late deceleration.

incoming beat to be chosen as PVC given that the previous beat was PVC. $\mathcal{U}(0,\,1)$ is the uniform distribution over the interval [0 1]. Gaussian parameters for the PVC beats were taken from Oster and Clifford (2013). Figure 6 shows an example of ectopic beats generated on the abdominal ECG mixture.

2.12. Modelling multiple pregnancies

The model can be generalised to multiple pregnancies by adding additional terms to equation (4). As an example in the case of twins:

$$\underline{\mathbf{s}}(t) = \mathbf{H}_m(t)\cdot\mathbf{R}_m(t)\cdot\underline{\mathbf{d}}_m(t) + \mathbf{H}_{f_1}(t)\cdot\mathbf{R}_{f_1}(t)\cdot\underline{\mathbf{d}}_{f_1}(t) + \mathbf{H}_{f_2}(t)\cdot\mathbf{R}_{f_2}(t)\cdot\underline{\mathbf{d}}_{f_2}(t) + \underline{\mathbf{w}}(t)\,,$$

where f_1 is used to designate the first foetus and f_2 the second. This generalisation allows the study of how source separation algorithms would perform in multiple pregnancies cases.

3. Discussion

The simulator introduced in this paper is not intended to be a substitute for clinical experimentation. In fact, it is meant to account for the inherent incompleteness of the current NI-FECG

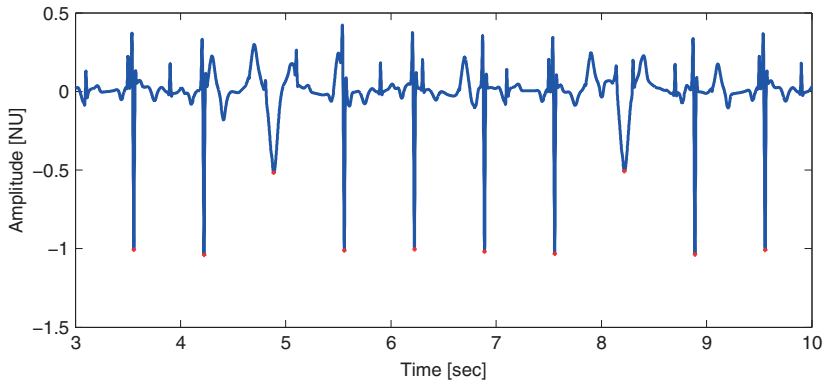

Figure 6. Example of ectopic beats generated on the abdominal ECG mixture.

databases and simulators. Its purpose is to facilitate the rapid stress-testing of NI-FECG algorithms under highly varied conditions, and with a complete gold standard. Essentially, the main purpose is to provide a common open-source tool for benchmarking extraction/detection algorithms. This tool allows the comparison between methods in the literature to extract the NI-FECG and FQRS complexes, which are a pre-requisite for clinical studies. We propose that the tool is used in order to provide a preliminary hurdle for stress testing algorithms and not to replace a data driven approach.

To date there is no study known to the authors that assessed the performance of the NI-FECG extraction algorithms with respect to electrode placement. In many instances, researchers made use of large arrays of electrodes or positioned the electrodes manually in order to get an acceptable extraction. The simulator presented can be used in order to better understand how electrode position, foetal position and orientation can influence the extraction algorithms.

The simulator can be used for generating a series of challenging scenarios such as contractions, fetal heart rate dips below the mother's heart rate, the effect of ectopy, cases of non-stationary mixes and the influence that the number of channels has on the performance of an algorithms (e.g. blind source separation). These analyses cases can be used to illustrate the limitations of existing NI-FECG extraction algorithms such as various template subtraction techniques and blind source separation (see for example the methods presented in (Behar *et al* 2014a, 2014b)).

The simulator also permits the testing of different conditions concomitantly. These conditions may have an impact on each other, e.g. an uterine contraction is expected to affect the foetal heart rate. Since the foetal heart rate response depends on the state of the foetus, there is no rule how this interaction should manifest. However, the ECG simulator allows the simulation of physiological and pathological conditions, which is the relevant aspect for FECG extraction methods. The user may adjust the simulator to embed rules to reflect this as they deem appropriate.

The volume conductor was chosen as a cylinder and the conduction properties were considered homogeneous. The vernix caseosa is a thin layer that forms around 28th–32nd weeks and dissolves in 37th–38th weeks in normal pregnancies (Stinstra 2001). It is highly non-conductive thus limiting successful NI-FECG extraction. There are few studies which describe the properties of the tissues involved in FECG conduction (Oostendorp *et al* 1989,

Stinstra and Peters 2002). The overall permittivity of the material between the fetal heart and the sensors also changes with gestational week, amount of placenta and presence of vernix caseosa. A more advanced modelling of how this thin layer affects permittivity would be required, thus the effects of such layer were not modelled in this paper. Nevertheless, an early and simple way of modelling this effect would be changing the value of the SNR_{fm} in order to decrease the FECG power into the mixture. However, the intention in this work was to keep the model simple, while realistic, to permit the evaluation of the effects that the physiological changes may have on the NI-FECG extraction algorithms. Thus our choice was driven by the need for simplicity and to avoid including overly specific quantities. Logical extensions of the simulator could include a more realistic volume conductor with inhomogeneous conduction properties. These extensions can easily be built upon the toolbox that we are releasing.

One of the limitations of the ECG simulator presented in this paper is that the morphology of the ECG cycle will vary linearly with HR (see equation (2) $-\dot{\theta} = \omega$). Although the PR, ST segments, the QRS complex and the T-wave are varying with HR (Hodges 1997), this variation is likely to be non-linear. One way of accounting for this problem would be to change the phase wrapping of the ECG model to be at least piece wise linear for each individual segment. Moreover, the noise sources provided by the NSTDB were only measured from one individual. Although our AR model allows to generate different noise time series, their power spectrum is roughly the same. As a consequence, in order incorporate more variability and improve the noise generator, it would be useful to have recordings from more individuals. Uterus activity could be better modelled with some real electrohysterography measurements. The simulator could be further improved by simulating atrial fibrillation in the MECG (Oster and Clifford 2013, Petrenas *et al* 2012). All these suggested additions to the simulator are easy to incorporate into the released version of the code.

4. Conclusion

In conclusion the foetal ECG synthetic simulator, *fecgsyn*, possesses the following features: realistic ECGs morphology using the Gaussian model, realistic noise, possibility to model HRV, rotation of the maternal and foetal heart axes with respect to respiration, foetus movement, ectopic beats and multiple pregnancy. The synthetic ECG simulator is a good tool for modelling realistic FECG-MECG mixtures and specific events such as abrupt HR increases in order to test signal processing algorithms on realistic data and for clinically important scenarios. We are releasing the code under an open source license (GNU general public licence) to encourage other users to test it and continue to improve the algorithms. The source code is available on PhysioNet at http://physionet.org/ (Clifford *et al* 2014b).

Acknowledgments

JB is supported by the UK Engineering and Physical Sciences Research Council, the Balliol French Anderson Scholarship Fund and MindChild Medical Inc. North Andover, MA. FA is financially supported by the Conselho Nacional de Desenvolvimento Tecnologico (CNPq - Brazil). JO is supported by the Royal Society under a Newton Fellowship, grant number 793/914/N/K/EST/DD PF/tkg/4004642 and the Wellcome Trust under grant number 098461/Z/12/Z for The University of Oxford Sleep and Circadian Neuroscience Institute (SCNi).

References

Behar J, Johnson A, Clifford G D and Oster J 2014a A comparison of single channel fetal ECG extraction methods *Ann. Biomed. Eng.* **42** 1340–53

Behar J, Oster J and Clifford G D 2014b Combining and benchmarking methods of foetal ECG extraction without maternal or scalp electrode data *Phys. Meas.* **35** 1569

Bousseljot R, Kreiseler D and Schnabel A 1995 Nutzung der EKG-Signaldatenbank CARDIODAT der PTB über das Internet *Biomed. Tech./Biomed. Eng.* **40** 317–8

Clifford G D, Behar J, Oster J and Johnson A 2014b IPM open source code *Physionet* (http://physionet.org/physiotools/ipmcode/)

Clifford G D, Nemati S and Sameni R 2010 An artificial vector model for generating abnormal electrocardiographic rhythms *Physiol. Meas.* **31** 595–609

Clifford G D, Silva I, Behar J and Moody G 2014 *Physiol. Meas.* **35** 1521

Dornan J, Ritchie J and Ruff S 1984 The rate and regularity of breathing movements in the normal and growth-retarded fetus *Int. J. Obstet. Gynaecol.* **91** 31–6

Feinstein N, Torgersen K L and Atterbury J 1993 *Fetal Heart Monitoring: Principles and Practices* (Dubuque: Kendall Hunt)

Goldberger A L, Amaral L A N, Glass L, Hausdorff J M, Ivanov P C, Mark R G, Mietus J E, Moody G B, Peng C K and Stanley H E 2000 PhysioBank, PhysioToolkit, and PhysioNet: components of a new research resource for complex physiologic signals *Circulation* **101** e215–20 (http://circ.ahajournals.org/cgi/content/full/101/23/e215)

Greer J J 2012 Control of breathing activity in the fetus and newborn *Comp. Physiol.* **2** 1873–88

Hodges M 1997 Rate correction of the QT interval *Card. Electrophysiol. Rev.* **1** 360–3

Kennedy H L, Whitlock J A, Sprague M K, Kennedy L J, Buckingham T A and Goldberg R J 1985 Long-term follow-up of asymptomatic healthy subjects with frequent and complex ventricular ectopy *New Engl. J. Med.* **312** 193–7

Leanderson S, Laguna P and Sörnmo L 2003 Estimation of the respiratory frequency using spatial information in the VCG *Med. Eng. Phys.* **25** 501–7

Malik M and Camm A J 1995 *Heart Rate Variability* (Armonk, NY: Futura)

McLeish K, Hill D L G, Atkinson D, Blackall J and Razavi R 2002 A study of the motion and deformation of the heart due to respiration *IEEE Trans. Med. Imag.* **21** 1142–50

McSharry P E, Clifford G D, Tarassenko L and Smith L A 2003 A dynamical model for generating synthetic electrocardiogram signals *IEEE Trans. Biomed. Eng.* **50** 289–94

Moody G B, Muldrow W E and Mark R G 1984 A noise stress test for arrhythmia detectors *Comp. Card.* **11** 381–4

Oostendorp T, Van Oosterom A and Jongsma H 1989 The effect of changes in the conductive medium on the fetal ECG throughout gestation *Clin. Phys. Physiol. Meas.* **10** 11

Oster J and Clifford G D 2013 An artificial model of the electrocardiogram during paroxysmal atrial fibrillation *Comp. Card.* **40** 539–42

Patterns I F 1999 Interpretation of the electronic fetal heart rate during labor *Am. Fam. Physician* **59** 2487–500

Petrenas A, Marozas V, Sornmo L and Lukosevicius A 2012 An echo state neural network for QRST cancellation during atrial fibrillation *IEEE Trans. Biomed. Eng.* **59** 2950–7

Sameni R, Clifford G D, Jutten C and Shamsollahi M B 2007 Multi-channel ECG and noise modeling: application to maternal and fetal ECG signals *EURASIP J. Adv. Signal Process.*

Silva I, Behar J, Sameni R, Zhu T, Oster J, Clifford G D and Moody G B 2013 Noninvasive fetal ECG: the physioNet/computing in cardiology challenge *Comp. Card.* **40** 149–52

Sobotka P A, Mayer J H, Bauernfeind R A, Kanakis C and Rosen K M 1981 Arrhythmias documented by 24 h continuous ambulatory electrocardiographic monitoring in young women without apparent heart disease *Am. Heart* J. **101** 753–9

Stinstra J G 2001 The reliability of the fetal magnetocardiogram *PhD Thesis* Universiteit Twente (http://doc.utwente.nl/35964/1/t000001d.pdf)

Stinstra J and Peters M 2002 The influence of fetoabdominal tissues on fetal ECGS and MCGS *Arch. Physiol. Biochem.* **110** 165–76

Stridh M and Sornmo L 2001 Spatiotemporal QRST cancellation techniques for analysis of atrial fibrillation *IEEE Trans. Biomed. Eng.* **48** 105–11

von Steinburg S P, Boulesteix A, Lederer C, Grunow S, Schiermeier S, Hatzmann W, Schneider K M and Daumer M 2012 What is the normal fetal heart rate? *PeerJ* **1** e82